Supporting Information

Dual-enhanced plasmonic biosensing for point-of-care sepsis detection

Lip Ket Chin[1,2], Jun-Yeong Yang[3], Benjamin Chousterman[4], Sunghoon Jung[3], Do-Geun Kim[3], Dong-Ho Kim[3], Seunghun Lee[3], Cesar M. Castro[1,5], Ralph Weissleder[1,5,6,7], Sung-Gyu Park[3*], Hyungsoon Im[1,6*]

[1] Center for Systems Biology, Massachusetts General Hospital, Boston, MA 02114, USA
[2] Department of Electrical Engineering, City University of Hong Kong, Kowloon, Hong Kong SAR
[3] Department of Nano-Bio Convergence, Korea Institute of Materials Science, 797 Changwondae-ro, Changwon 51508, Republic of Korea
[4] Département d'Anesthésie-Réanimation, Hôpitaux Universitaire Saint-Louis, 75010, Paris, France
[5] Cancer Center, Massachusetts General Hospital, Boston, MA 02114, USA
[6] Department of Radiology, Massachusetts General Hospital, Boston, MA 02114, USA
[7] Department of Systems Biology, Harvard Medical School, 200 Longwood Ave, Boston, MA 02115, USA

*Corresponding authors:
Hyungsoon Im (im.hyungsoon@mgh.harvard.edu)
Sung-Gyu Park (sgpark@kims.re.kr)

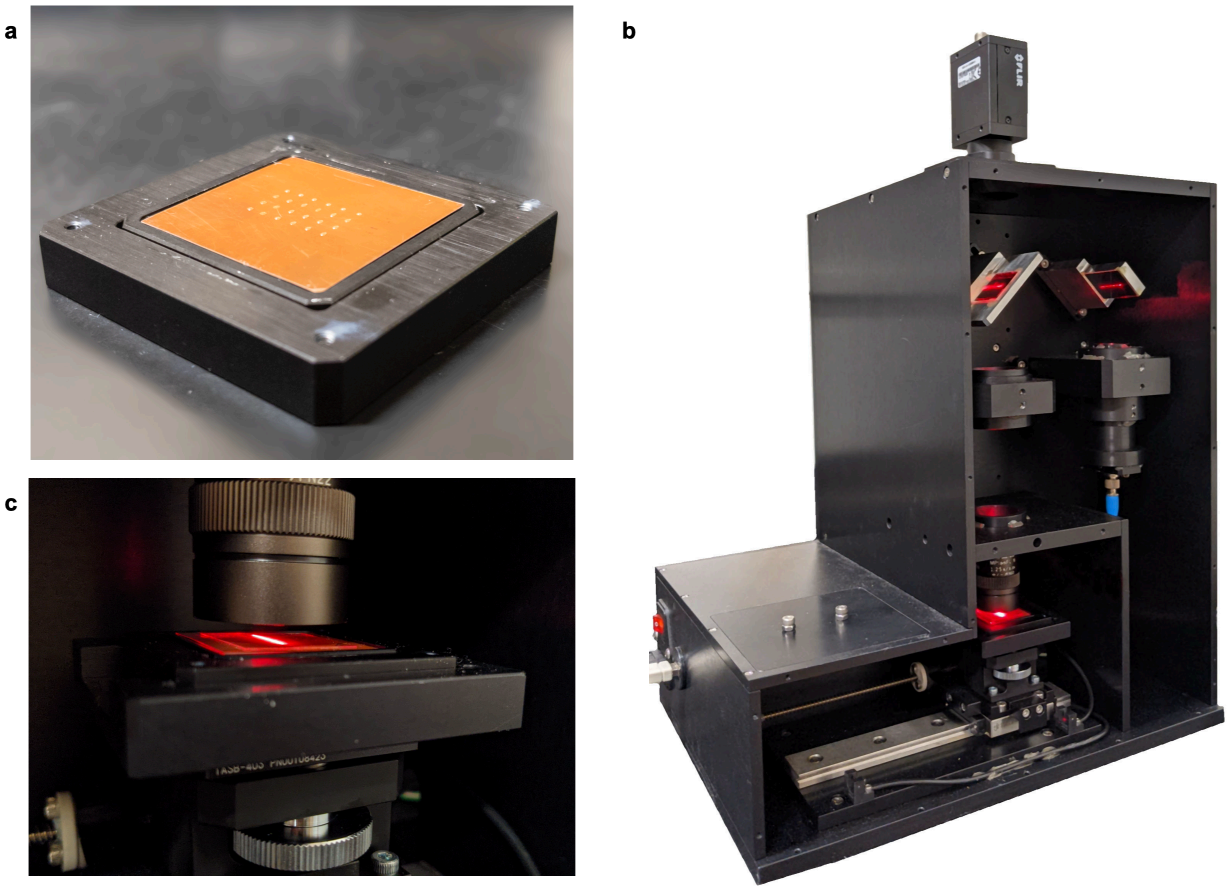

Fig. S1: In-house chip and system development. (a) Multiple spotted capturing antibodies on NPOD chip for multiplexed measurement. **(b)** Line-scanning laser imaging system. **(c)** Zoom-in view of the NPOD chip being scanned by the line laser.

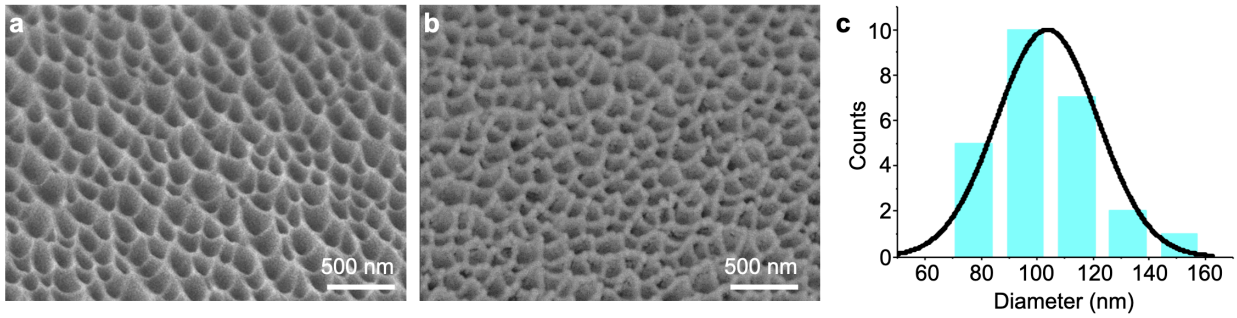

Fig. S2: Characterization of PEN and Au nanodimples. (a-b) SEM images of nanodimple structures in a polyethylene naphthalate (PEN) film (a) before and (b) after 100 nm-thick gold deposition. **(c)** Size distributions of Au nanodimples.

Fig. S3: Transmission electron micrographs (TEMs) of Au nanoparticles formed on the

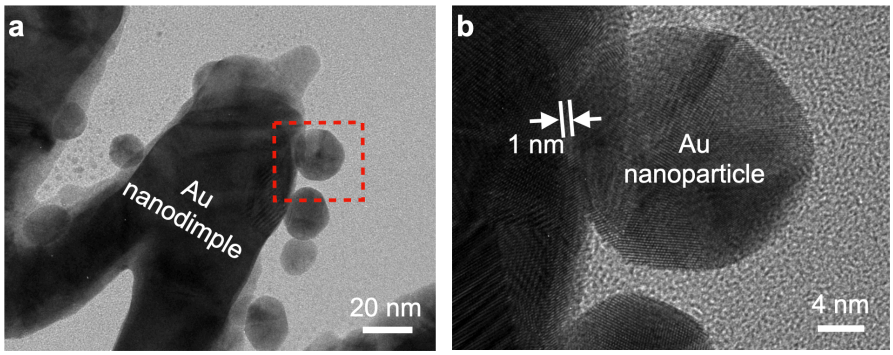

nanodimple structure. (a) TEM images of NPOD nanostructures after 10 nm Au deposition on the PFDT-coated Au nanodimple structures. The diffused Au adatoms formed the spherical nanoparticles at the defect sites of the PFDT-coated Au nanodimple surface. **(b)** A high-resolution TEM image is a zoomed-in image of the red box area in (a).

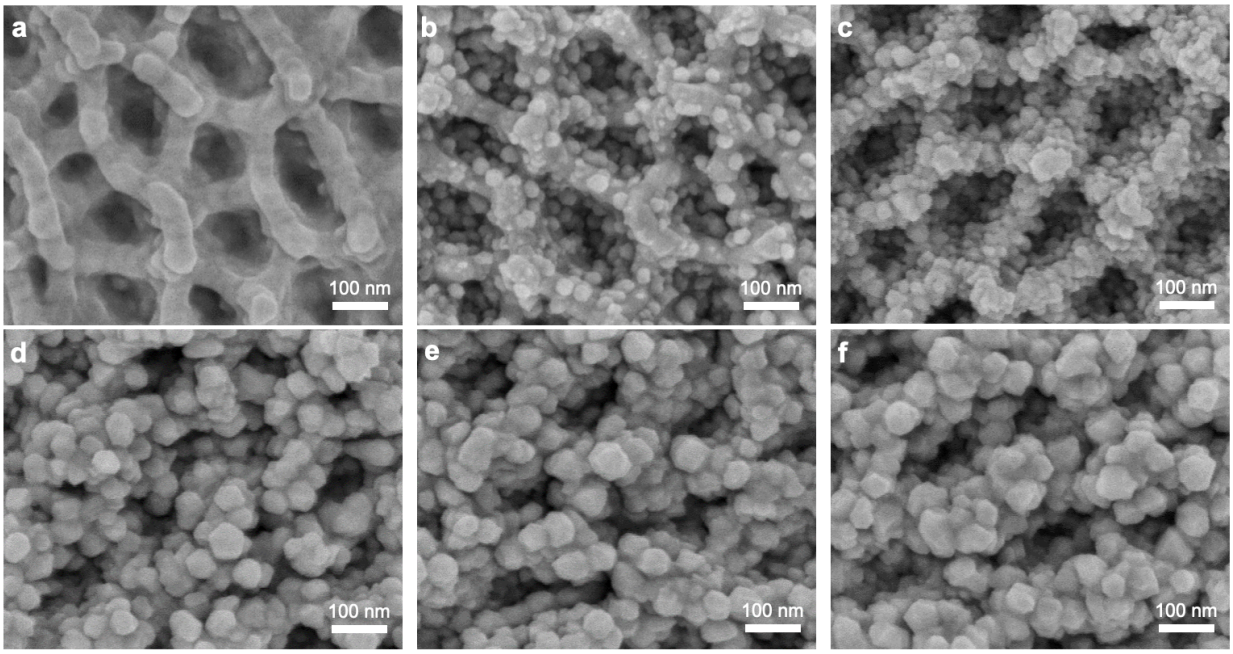

Fig. S4: Au Nanoparticle on nanodimple substrates with varying thicknesses of Au deposited on 1H,1H,2H,2H-perfluorodecanethiol (PFDT)-coated gold nanodimple structures. (a) 0 nm. **(b)** 20 nm. **(c)** 40 nm. **(d)** 60 nm. **(e)** 80 nm. **(f)** 100 nm.

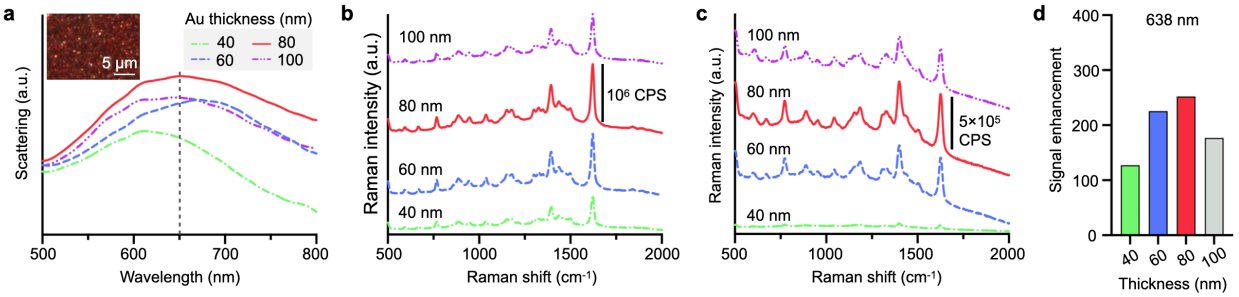

Fig. S5: Optical characteristics of NPOD chip. (a) Scattering light spectra of NPOD Au chips prepared by depositing different Au thicknesses on PFDT-coated Au nanodimples. The resonant peak (650 nm) was represented with a vertical gray dashed line. Raman spectra for methylene blue on various plasmonic NPOD chips at an incident wavelength of **(b)** 638 nm and **(c)** 785 nm. **(d)** Bar chart graph for signal enhancement of NPOD chips normalized by bare signal at incident wavelengths of 638 nm and 785 nm.

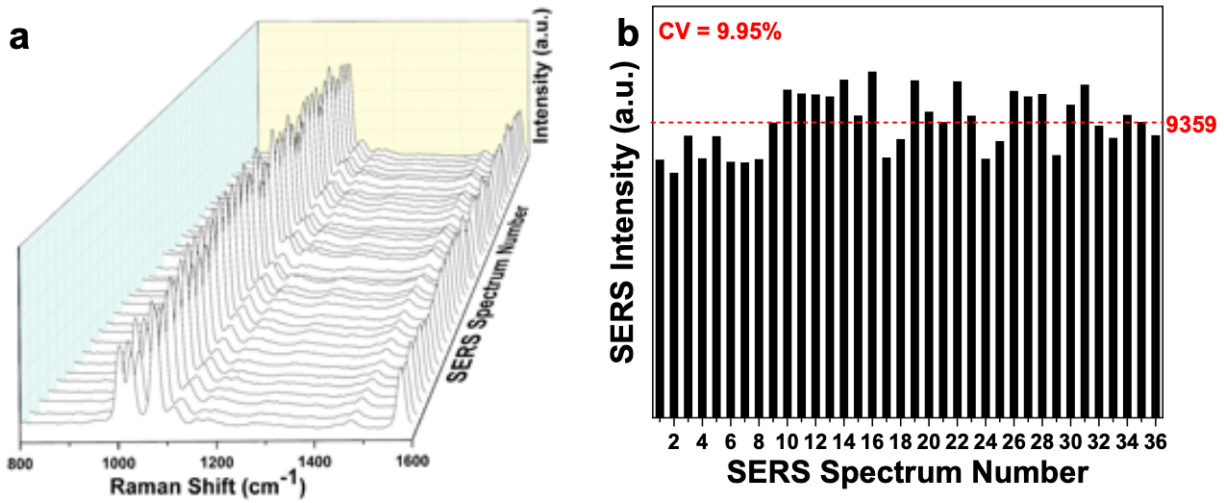

Fig. S6: SERS measurements of benzenethiol (BT)-treated NPOD substrates. (a) SERS spectra of BT were measured from 36 random spot measurements across a 90 mm × 90 mm area. **(b)** Variations in the distribution of SERS intensities at 1075 cm^{-1}, showing the coefficient of variation less than 10%.

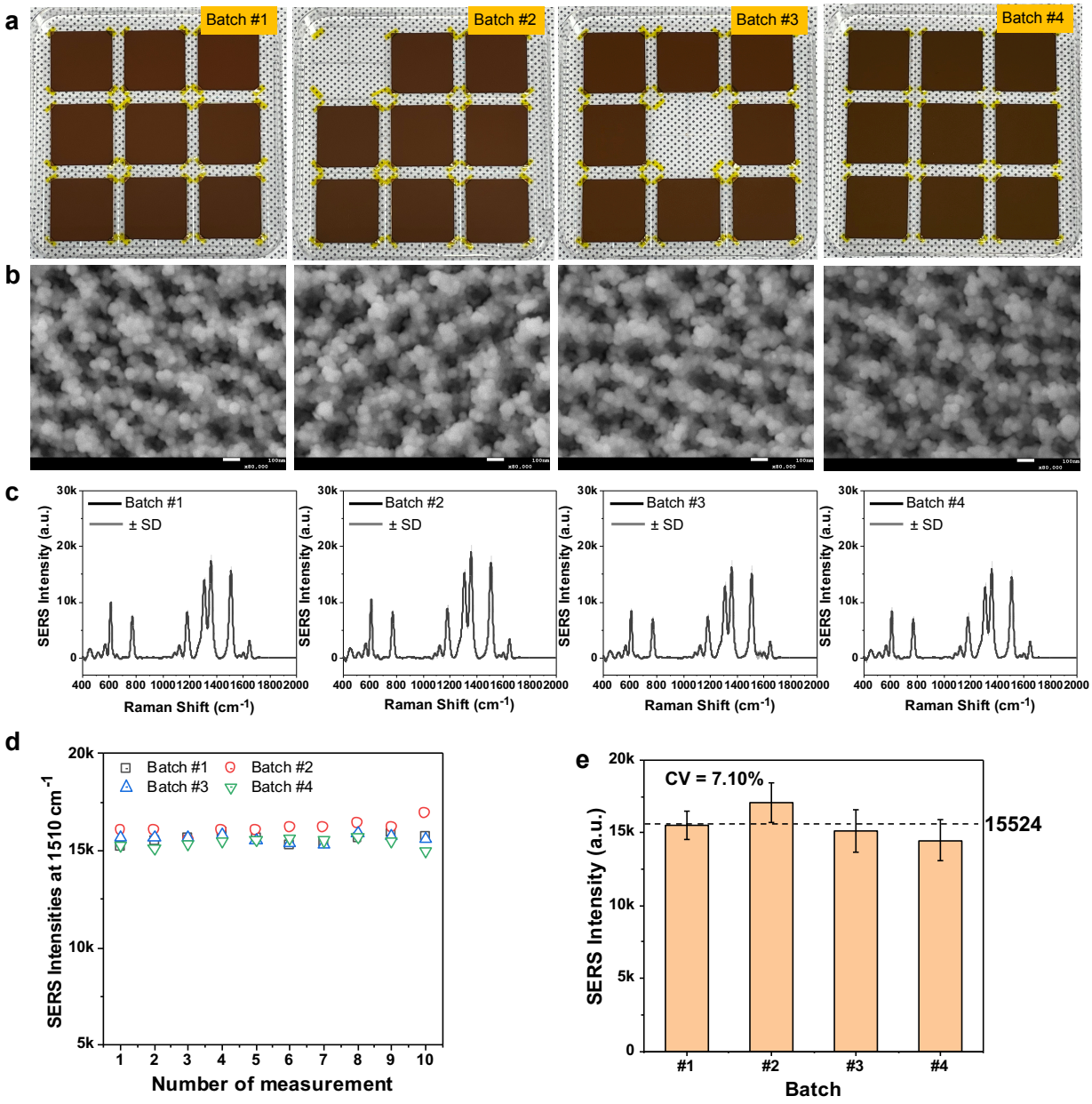

Fig. S7: Batch-to-batch reproducibility of NPOD substrates. (a) Photographs of NPOD substrates fabricated in four different batch times. **(b)** Corresponding SEM images of a randomly selected chip in the batches in (a). **(c)** Reproducibility data of SERS signals. 1 μM R6G SERS signals were measured on four different NPOD substrates from different batches. The black spectra represent the average of ten repeated spectra measurements for each substrate. The gray shades denote standard deviations (±SD) of the measured spectra. **(d)** SERS intensities of R6G peak at 1510 cm^{-1} for all ten spectra measured from the four substrates. **(e)** Average intensities and standard deviations of the 1510 cm^{-1} peak for substrates from four different batches.

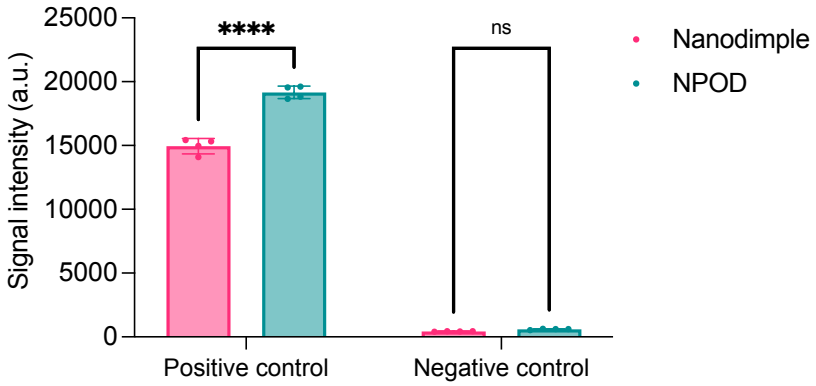

Figure S8. Comparison between Au nanodimple arrays without spiked nanoparticles (nanodimple) and with spiked nanoparticles (NPOD). Positive fluorescence signals increased by about 30% (Šídák's multiple comparison test, $P < 0.0001$), while there is no significant difference in the background signal from a negative control sample ($P = 0.80$).

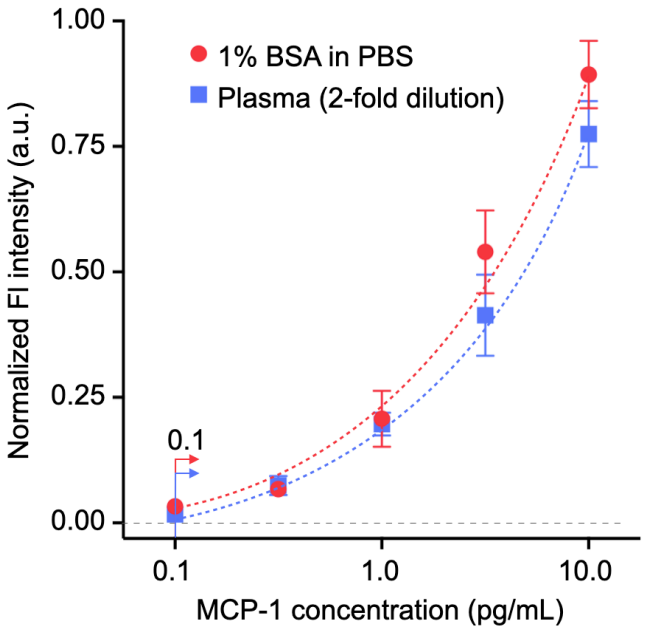

Fig. S9: Comparison of the DuPLUS assay for detecting MCP-1 spiked in 1% BSA in PBS (red) and diluted human plasma (blue)

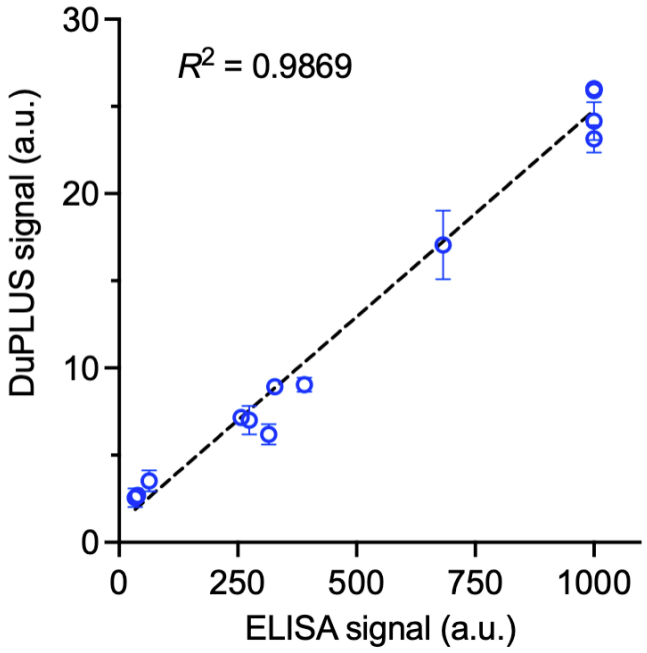

Fig. S10: Correlation of IL-6 measurements on septic samples between DuPLUS assay and commercial fluorescence-based ELISA kits. Linear regression analysis was performed using Prism 9 for the fitted line, and the R^2 value represents the goodness of fit (p-value < 0.0001). The Spearman correlation coefficient was r = 0.9674 (p-value < 0.0001).

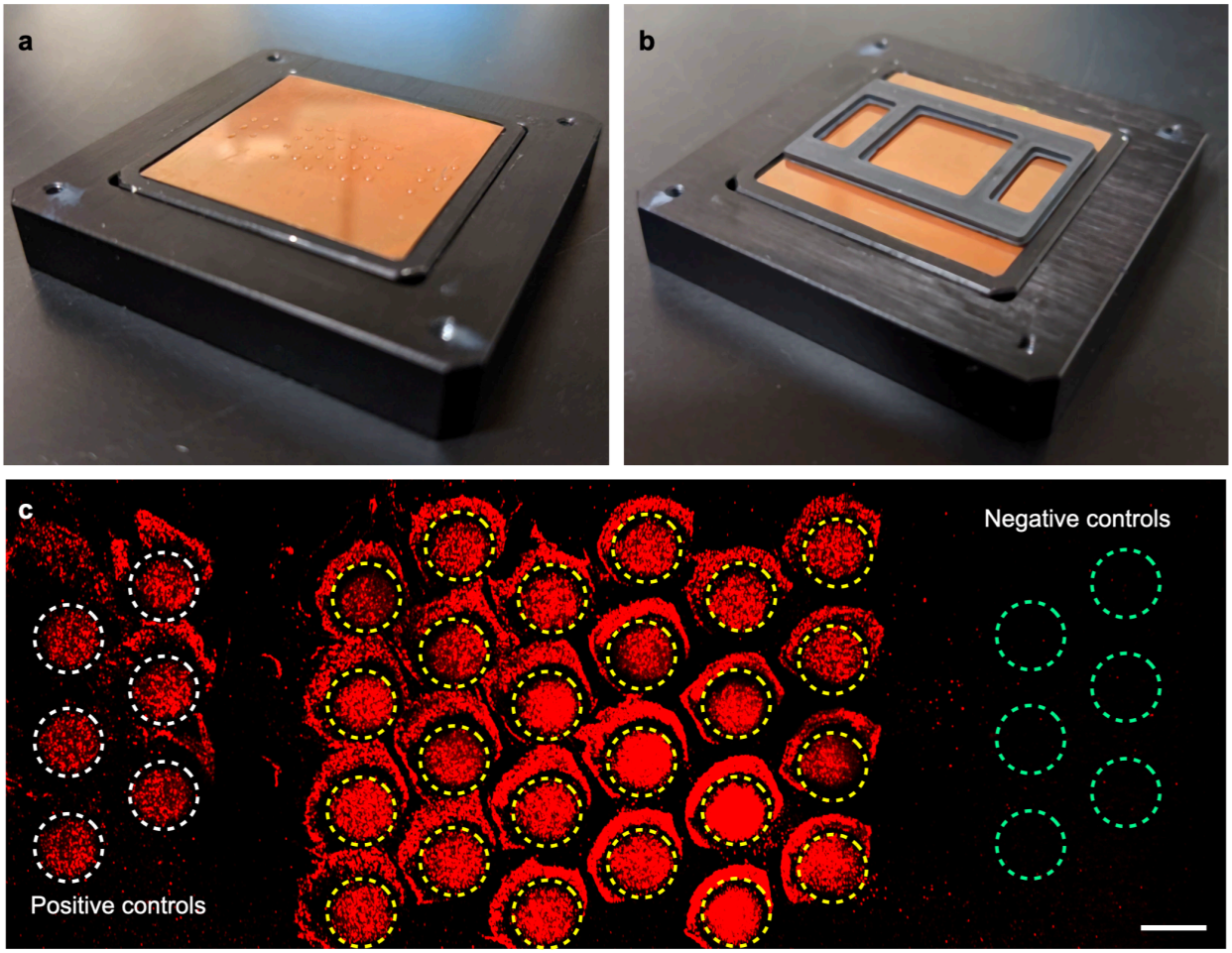

Fig. S11: Integrated open reservoir fluidic chip. (a) Multiple spotted capturing antibodies for multiplexed measurement. **(b)** Integrated open reservoir fluidic chip. **(c)** A scanned image of the multiplexed cytokines, including positive and negative controls. Scale bar: 1.5 mm.

Table S1. Surface energy of spacer materials

Type	Material	Surface energy (J/m^2)	
Dielectric	SiO_2	0.054	(a)
	Al_2O_3	0.97	(b)
	TiO_2	0.033	(c)
Polymer	PVA	0.061	(d)
	Teflon (PTFE)	0.019	(e)
	PFDT	0.015	In this study
Metal	Au	1.54	In this study

(a) Di, C.; Yu, G.; Liu, Y.; Guo, Y.; Sun, X.; Zheng, J.; Wen, Y.; Wang, Y.; Wu, W.; Zhu, D. Effect of dielectric layers on device stability of pentacene-based field-effect transistors. *Phys. Chem. Chem. Phys.* **2009**, *11*, 7268–7273.

(b) Park, S.-G.; Xiao, X.; Min, J.; Mun, C.; Jung, H. S.; Giannini, V.; Weissleder, R.; Maier, S. A.; Im, H.; Kim, D.-H. Self-Assembly of Nanoparticle-Spiked Pillar Arrays for Plasmonic Biosensing. *Adv. Funct. Mater.* **2019**, *29*, 1904257.

(c) Liu, L.; Bhatia, R.; Webster, T. J. Atomic layer deposition of nano-TiO2 thin films with enhanced biocompatibility and antimicrobial activity for orthopedic implants. *Int. J. Nanomed.* **2017**, *12*, 8711–8723.

(d) Kang, S. B.; Kwon, K. C.; Choi, K. S.; Lee, R.; Hong, K.; Suh, J. M.; Im, M. J.; Sanger, A.; Choi, I. Y.; Kim, S. Y.; Shin, J. C.; Jang, H. W.; Choi, K. J. Transfer of ultrathin molybdenum disulfide and transparent nanomesh electrode onto silicon for efficient heterojunction solar cells. *Nano Energy* **2018**, *50*, 649–658.

(e) Huang, S.; Wan, Y.; Ming, X.; Zhou, J.; Zhou, M.; Chen, H.; Zhang, Q.; Zhu, S. Adhering Low Surface Energy Materials without Surface Pretreatment via Ion−Dipole Interactions. *ACS Appl. Mater. Interfaces* **2021**, *13*, 41112–41119.

Table S2. Demographic summary of septic patients

Variables	Total population	Value	No of survivors in ICU	Value	No of non-survivors	Value
Age (years)	15	67 (61 - 73)	12	65 (59 - 74)	3	71 (64 - 73)
Female (%)	15	9 (60 %)	12	8 (67 %)	3	1 (33 %)
Length of stay in ICU (days)	15	14 (8 - 27)	12	18 (8 - 28)	3	13 (5 - 14)
Charlson score	15	2 (1 - 3)	12	2 (0 - 2)	3	4 (1 - 6)
SAPS II score	15	59 (54 - 74)	12	58 (54 - 70)	3	74 (58 - 101)
SOFA score	13	11 (10 - 13)	11	12 (10 - 13)	2	11 (11 - 11)
Hypertension	15	6 (40 %)	12	6 (50 %)	3	0 (0 %)
Chronic heart failure	15	2 (13 %)	12	2 (17 %)	3	0 (0 %)
Diabetes mellitus	15	4 (27 %)	12	4 (33 %)	3	0 (0 %)
Chronic obstructive pulmonary disease	15	4 (27 %)	12	3 (25 %)	3	1 (33 %)
Chronic renal disease	15	2 (13 %)	12	2 (17 %)	3	0 (0 %)
Active or recent malignant Cancer	15	2 (13 %)	12	1 (8 %)	3	1 (33 %)
Renal replacement therapy	15	10 (67 %)	12	8 (67 %)	3	2 (67 %)

Table S3. Demographic summary of healthy controls

Variables	Total population	Value
Age (years)	5	37 (28 - 46)
Female (%)	5	2 (40%)

Table S4. Threshold levels for cytokines and chemokine.

Target	Threshold (pg/mL)
IL3	15
TNFa	5
IL6	8
IL10	4
IL1b	2
MCP1	75